

# Multi imaging-based beam shaping for ultrafast laser-material processing using spatial light modulators

Jiangning Li<sup>a</sup>, Yue Tang<sup>a\*</sup>, Zheng Kuang<sup>a</sup>, Joerg Schille<sup>b</sup>, Udo Loeschner<sup>b</sup>, Walter Perrie<sup>a</sup>, Dun Liu<sup>c</sup>, Geoff Dearden<sup>a</sup> and Stuart Edwardson<sup>a</sup>

- a. Laser Group, School of Engineering, University of Liverpool, Brownlow Street, Liverpool L69 3GQ, UK
- b. Laserinstitut Hochschule Mittweida, Technikumplatz 17, 09648 Mittweida, Germany
- c. School of Mechanical Engineering, Hubei University of Technology, Wuhan 430068, China

\* Corresponding author. *E-mail address:* hsytan10@liverpool.ac.uk

## Abstract

An imaging based beam shaping technique combined with parallel beam processing has been demonstrated. Binary and intensity masks have been designed and applied on phase only spatial light modulator (SLM) to shape the input laser beam in the desired profile and intensity distribution. A second SLM with a computer generated hologram (CGH) applied was used to split the incident picosecond laser beam. Hence, the laser beam was effectively converted to required target shape, intensity distribution and a separated pattern then reconstructed at the image plane of a focusing lens. The machined footprints on a polished Titanium (Ti6Al4V) substrate accurately match the desired beam in shape and depth distribution.

Keywords: Laser beam shaping; Laser parallel beam processing; Spatial light modulator.

## 1. Introduction

Ultrafast lasers are increasing in precision manufacturing as it can be regarded as a high quality tool for micro-processing on various materials like metals [1] [2], semiconductors [3] and dielectrics [4]. Most of the laser processing used Gaussian beams and more and more researcher investigated the laser processing with different shaped laser beams and intensity [5] [6]. A single spatial light modulator (SLM) has been used for beam shaping with computer generated holograms (kinoform) under high input power [7].

Parallel processing using diffractive multiple beams generated by a spatial light modulator has been studied to improve the throughput and efficiency of ultrafast laser processing [8] [9]. By synchronisation with a scanning galvo,

parallel processing shows more flexibility and potential in industrial applications [10] [11].

Another characteristic of ultrafast laser material processing is that the shape of the ablated area is very close to the laser beam intensity distribution due to a well defined ablation threshold coupled with the absence of melt. A number of beam shaping studies have been motivated by this approach [12]. The use of amplitude mask projection with diffractive optical elements (DOEs) [13] and deformable mirrors [14], demonstrate effective shaping of ultrashort pulse laser beams. For example, multiple annular beams were generated at the focal plane for high speed picosecond laser micro-drilling of stainless steel foil with diffractive axicon phases using a spatial light modulator (SLM) [15].

An interesting novel imaging-based amplitude beam shaping technique using a spatial light modulator has been recently demonstrated where arbitrary shapes and flat top beam can be obtained by grey level geometric masks at the diffraction near-field then reconstructed at an imaging plane with a size comparable with the beam waist at the focal plane [16] [17].

In this paper, beam shaping combined with parallel processing to generate multiple

shaped beams is presented with two SLMs for the first time. Both binary and intensity grey level geometric mask have been used to fully shape the ultrashort pulsed input laser beam to the outline profile and intensity distribution. After a long beam path, a second SLM has been used for beam splitting by computer generated hologram (CGH). The multiple beam shapes were then reconstructed at the image plane of an f-theta lens ( $f \sim 100\text{mm}$ ).

## 2. EXPERIMENTAL AND METHODOLOGY

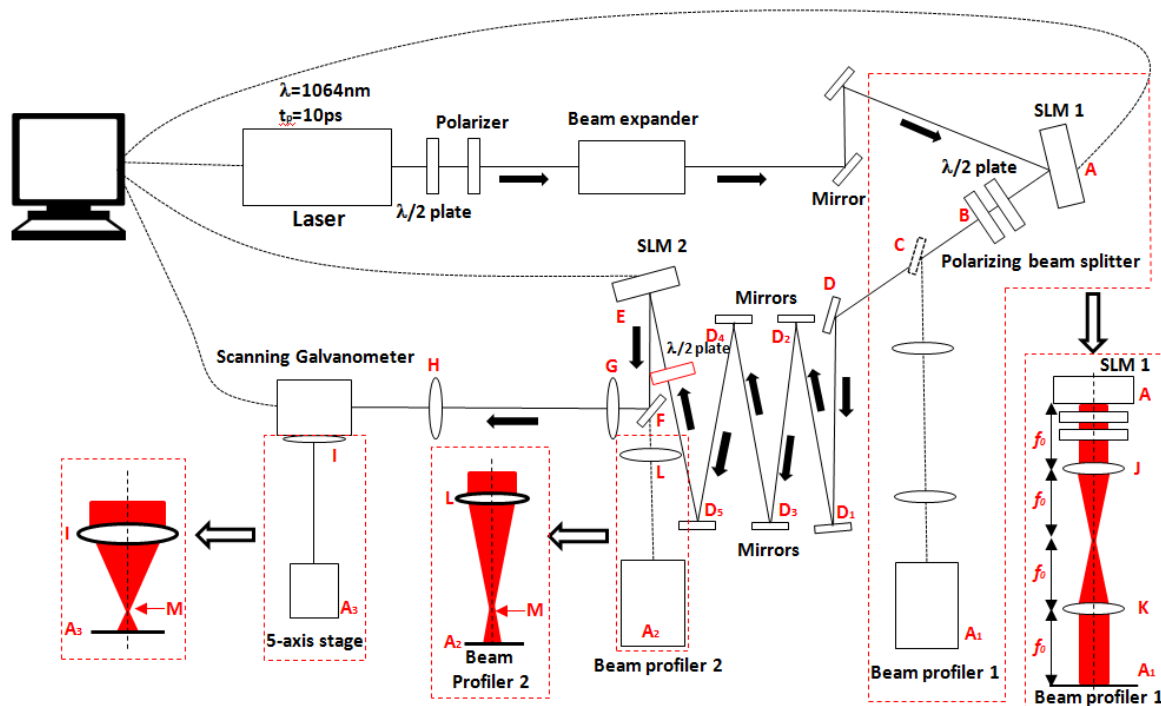


Figure 1 Experimental setup

### 2.1 Experimental setup

A schematic of the experimental setup is shown in Figure 1. The laser source is a custom made Nd:VAN seeded regenerative amplifier (High-Q IC-355-800ps, Photonic Solutions) with output pulse duration  $\tau = 10\text{ps}$ , wavelength  $\lambda=1064\text{nm}$ , repetition rate  $\text{PRF}=10\text{kHz}$  and beam diameter  $d \approx 2.7\text{mm}$ . The beam passes through a half wave plate and polarizer used for adjusting both power and polarization direction ( $45^\circ$ ), a beam expander ( $M \approx \times 3$ ) and directed by two plane

mirrors to the first reflective, liquid crystal SLM1 (Hamamatsu X13138-5785,  $1280 \times 1024$  pixels, fill factor 96%) at low angle of incidence  $< 10^\circ$ .

The SLM1 (A) contains a parallel-aligned liquid crystal layer. An active matrix circuit is formed on the silicon substrate for applying appropriate voltages to pixel electrodes. Pure phase modulation of the incident light can be achieved when aligning the incident polarization parallel to the orientation of the liquid crystal while polarisation modulation

results when incident polarisation is 45°. A polarizing beam splitter (B) combined with a half wave plate were placed after SLM1 to modulate the laser beam intensity for the onward beam shape.

When observing the beam profile after shaping, the beam was reflected by a flip mirror (C) and 4f system with two positive lenses (focal length:  $f_0=200\text{mm}$ ) to reach beam profiler 1 (Thorlabs BC106-VIS). When processing, the flip mirror was removed and the beam traversed a long beam path ( $L = 4.3\text{m}$ ) by multiple reflected mirrors ( $D - D_5$ ) to reach the second reflective phase only SLM2 (Hamamatsu X10468-03, 800x600 pixels, fill factor 98%).

Before SLM2, a half wave plate has been added to modulate the polarization horizontal relative to SLM2 for the onward multiple beam generation. After the SLM2, the beam was reflected by a flip mirror (F) to a scanning galvanometer (Nutfield XLR8-10) and f-theta focusing lens ( $f_{f,\theta}=100\text{mm}$ ). Lens G and lens H consists a 4f-system. M is the focal point. Machining samples were mounted on a five-axis ( $x,y,z,u,v$ ) motion control stage (Aerotech) placed under the f-theta lens. When observing the beam profile after beam splitting, the flip mirror was removed to let the beam pass through a positive lens (focal length:  $f_0=750\text{mm}$ ) to reach the second CCD camera and beam profiler (Spiricon SP620U) placed at the image plane of the lens. Hence, the desired beam shape with multi-beams could be observed before material processing.

## 2.2 Beam shaping using a SLM1

The setup of the intensity modulation system contains a 45° linear polarized incident laser beam, a Hamamatsu X13138-5785 SLM with a half wave plate and a polarizer. The setup can be expressed as a Jones vector noted  $J(x,y)$ , where x and y are the horizontal and vertical

coordinates across the beam profiles. A full derivation for the resulting electric field amplitude using the optical properties of the setup gives:

$$J(x,y) = \begin{pmatrix} 1 & 0 \\ 0 & 0 \end{pmatrix} \times \begin{pmatrix} \cos 2\theta & \sin 2\theta \\ \sin 2\theta & -\cos 2\theta \end{pmatrix} \times \begin{pmatrix} e^{i\phi(x,y)} & 0 \\ 0 & 1 \end{pmatrix} \times \begin{pmatrix} \frac{1}{\sqrt{2}} \\ \frac{1}{\sqrt{2}} \end{pmatrix} \quad (1)$$

where  $\phi(x,y)$  related to grey level is the phase delay induced with the first SLM and  $\theta$  is the angle of the fast axis of half wave plate. The intensity of the output can be derived from Equation (1) given by  $J(x,y)^2$

$$I = \frac{1}{2} \begin{pmatrix} \cos 2\theta e^{-i\phi(x,y)} + \sin 2\theta & 0 \\ \cos 2\theta e^{i\phi(x,y)} + \sin 2\theta & 0 \end{pmatrix} = \frac{1}{2} + \frac{1}{2} \sin 4\theta \cos \phi \quad (2)$$

where  $I$  is the transmission efficiency. When  $I = 1$  the laser beam is passed through the polarizing beam splitter (B) without loss, when  $I = 0$ , the polarizing beam splitter directs all the intensity to a beam dump at a side port. As shown in Equation (2), when  $\theta = \frac{3}{8}\pi$ ,  $I = \frac{1}{2} - \frac{1}{2} \cos \phi$ , which means that using this method, the transmitted relative intensity can be adjusted from 0 to 1 (as with the incident beam), see Figure 2. The measured values in figure 2 have been taken from beam profiler 1. Variable grey level values on SLM1 correspond to different transmitted powers at  $A_1$ . Each measured power can then divided by the measured maximum power. The transmission efficiency curve can then be plotted. The theoretical values are based on the calibration data for the device from the manufacturer. Based on the equation  $I = \frac{1}{2} - \frac{1}{2} \cos \phi$ , the corresponding theoretical curve can be extracted.

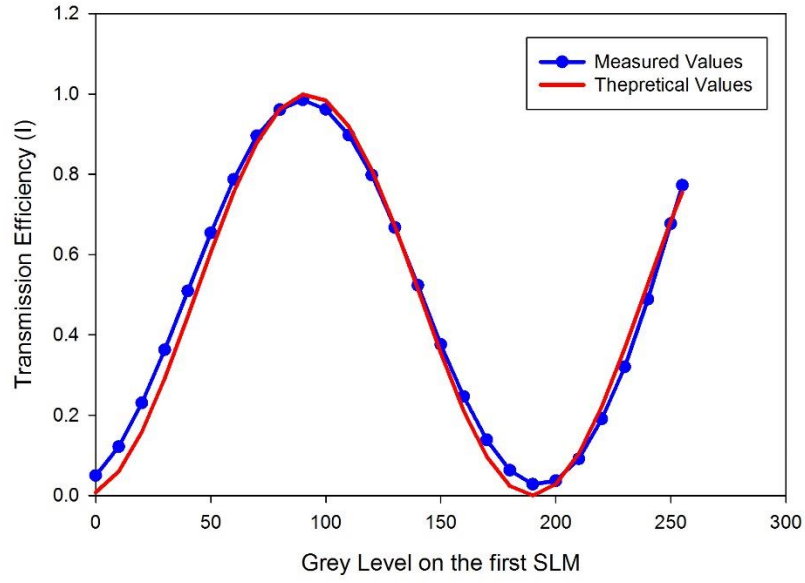


Figure 2 Measured and theoretical transmission efficiency through analyser versus the grey level applied on the first SLM. Theoretical values (red line) are calculated with equation:  $I = \frac{1}{2} - \frac{1}{2} \cos \phi$ .

### 2.3 Outline shape and intensity distribution design

The measured values have been used for beam shaping. Both the binary and grey level masks were created and applied to the first SLM. With a binary mask, the outline of the input beam can be changed into any required shape, while the intensity distribution will remain same as the original Gaussian distribution. However, with a grey level mask added, the intensity distribution can also be modified. For example, if the target beam has a flat top distribution with intensity  $Y(m,n)$ , the required intensity  $Y(m,n)$  should be proportional to the transmission efficiency  $I(m,n)$  multiplied by original near Gaussian intensity distribution  $O(m,n)$  measured from the beam profiler and edited using Matlab to yield constant spatial intensity. This is given in Equation (3) where  $\alpha$  is a factor to normalize the required intensity  $Y(m,n)$  between 0 and 1.

$$Y(m,n) = \alpha \times I(m,n) \times O(m,n) \quad (3)$$

$I = I(m,n)$  where  $(m,n)$  is pixel position. Thus, the  $Y$  can be achieved based on pixel position of shaped area.

The equation for (I) can be derived from Figure 2:

$$I(m,n) = \frac{1}{2} - \frac{1}{2} \cos\left(\frac{2\pi}{190} \times [GL]\right) \quad (4)$$

where  $[GL]$  is the grey level of a given point in the  $300 \times 300$  matrix and the value is displayed on the SLM. The measured corresponding grey level on SLM1 to  $2\pi$  phase is 190. As the input polarization is  $45^\circ$ , the output linear polarization state can therefore be rotated with the grey level. The induced phase-delay has been founded linearly related to  $[GL]$  [18]. By combining equation (1) and (2), we can derive:

$$[GL] = \frac{190}{2\pi} \arccos\left[\left(\frac{Y(m,n)}{\alpha O(m,n)} - \frac{1}{2}\right) \times 2\right] \quad (5)$$

Based on equation (5), an intensity mask which can shape the original beam into a flat top distribution as an example can be created.

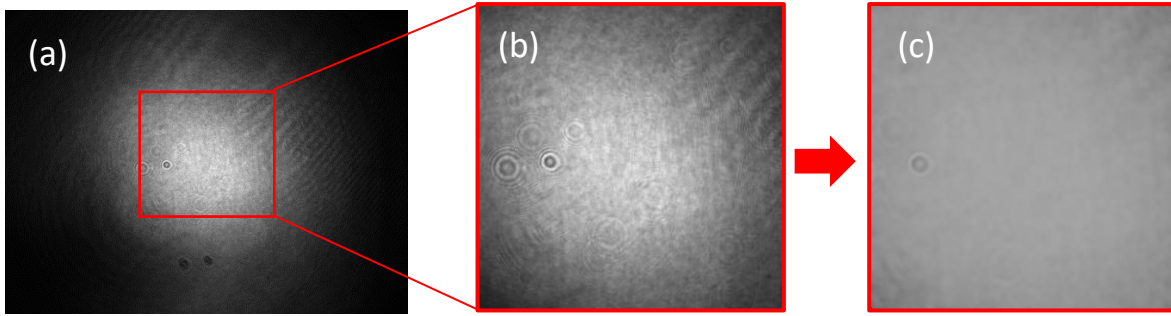


Figure 3 Original and shaped beam profiles (a) Original 2D profile in grey scale.(b) Shaped area of interest (300×300 pixels). (c) Grey level mask generated by Matlab

As shown in Figure 3, the original beam profile was taken by a beam profiler and read using Matlab. Figure 3 (b) shows the square shaped area which has a side length of 300 pixels ( $\approx 2\text{mm}$ ) and Figure 3 (c) shows the grey level

mask calculated by pixels based on Equation (5). By applying the grey level mask on the SLM1, a flat top beam can be achieved as the original phase has been modified with the optimal  $2\pi$  phase values.

#### 2.4 Beam splitting using additional Spatial Light Modulator, SLM2

Diffractive multi-beam patterns can be generated using a second spatial light modulator (SLM2, Hamamastu X10468-03, 800X600pixels, fill factor 98%),on which computer generated holograms (CGHs) are displayed. An iterative Fourier-transform

algorithm calculated by the Hamamatsu LCoS control software has been applied for multi-beam output. The used CGH is a multilevel phase-only hologram and SLM2 is working in a phase-only regime. The input beam polarization has been modulated to horizontal with respect to the long axis of SLM2 with a half wave plate.

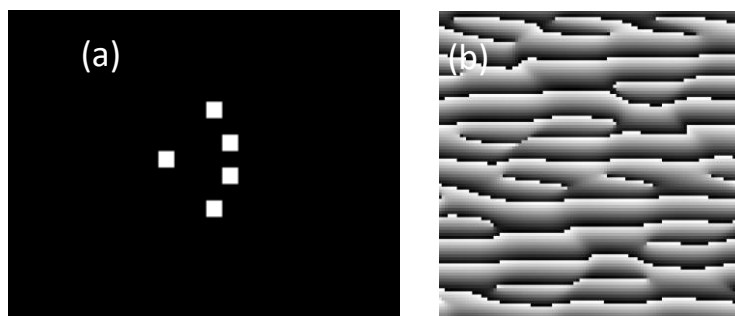


Figure 4 Target pattern and its calculated CGH using Hamamatsu software. (a) Target pattern. (b) Computer generated hologram.

As shown in Figure 4 (a), a pattern of five points was input into the software and the corresponding hologram was generated. As this the CGH on SLM 2 is a Fourier hologram, thus plane A2 and A3 are the Fourier transform planes of plane E of SLM2, therefore an output of five spots will be

generated at the focal plane after passing the focusing lens. In this case, the spots will retain the desired shape and intensity distribution.

## 2.5 Shaping reconstruction at the imaging plane of a focusing lens

As shown in Figure1, the generated mask has shaped the incident beam in the near field after the SLM at A. This shape was reconstructed after the 4-f optical system at beam profiler, A<sub>1</sub> for observation. In addition, this was also reconstructed after a focusing lens at beam profiler A<sub>2</sub> for observation of beam splitting performance. The modulated beam then reaches the F-theta lens and is reconstructed at the imaging plane. As shown in Figure 1, there are five mirrors, D<sub>1</sub>-D<sub>5</sub>, added to the beam path to significantly increase the distance from the first SLM to the focusing F-theta lens, i.e. the object distance. The purpose of this was to reconstruct the shape to a small size comparable to the beam waist. The position of the imaging plane A<sub>3</sub> can be calculated, based on the thin lens imaging equation below.

$$\frac{1}{u} + \frac{1}{v} = \frac{1}{f} \quad (6)$$

where  $u \approx 4300mm$  is the object distance, while  $f = 100mm$  is the focal length of the F-theta lens and  $v$  is the image distance, the distance from the F-theta lens(G) to image plane(A<sub>3</sub>). Hence, we obtain,

$$v = \frac{fu}{u-f} \approx 102.04mm \quad (7)$$

$$d = v - f = 2.04mm \quad (8)$$

where  $d$  is the image offset from lens focal plane. The magnification factor of this

system is  $M \approx 1/45$ , therefore, when a 300 pixel side length mask is applied, and the original expanded size is approximately 2mm, the diameter of the reconstructed beam at A<sub>3</sub> can be calculated to be approximately 41 $\mu$ m.

Since both the shape and multi-beam pattern require to be observed, a similar method is used at a second beam profiler A<sub>2</sub>. A positive lens (focal length:  $f_0=750mm$ ) was placed after the second SLM and the beam profiler was placed at the imaging plane.

## 3 RESULTS AND DISCUSSION

### 3.1 Beam-shaping results observed by CCD Cameras at A<sub>1</sub> and A<sub>2</sub>

Referring to Figure 5 and Figure 6, the top line of images shows the results of beam shaping using the first SLM. By applying a square or a star shape binary mask, the corresponding beam shape can be observed at A<sub>1</sub>. The binary mask only shaped the outline profile but left the inside intensity distribution (Gaussian) unchanged. The lower line shows the results of beam splitting by SLM2. A square shape beam was separated into four in Figure 5, while a star shape beam was separated into five in Figure 6. Both modulated outputs carry the desired beam shape with parallel beams. The intensity of their central area can be seen to be higher due to the Gaussian nature of the original beam.

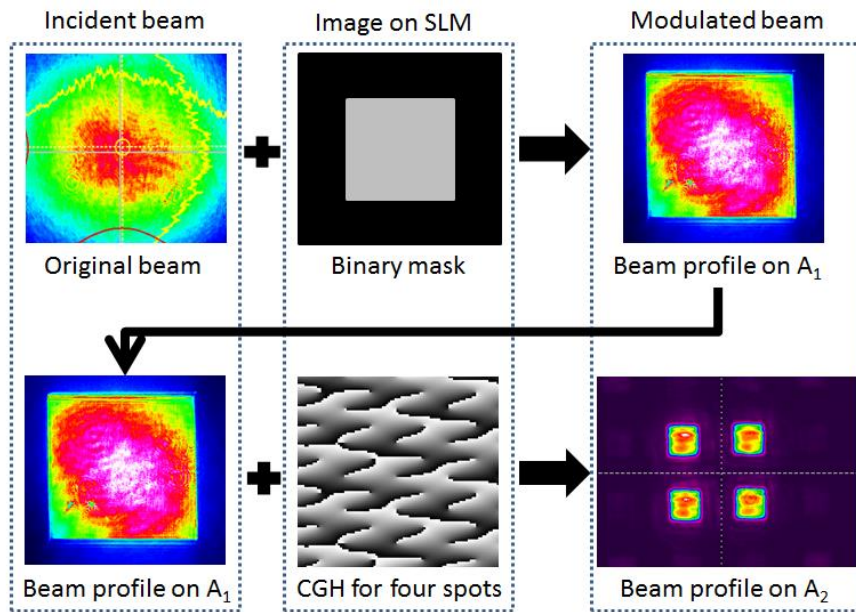


Figure 5 Four square beams. Top line: the original distribution plus a binary mask to achieve a square shape beam at  $A_1$ . Lower line: the square shape beam plus CGH to achieve four square beams at  $A_2$ .

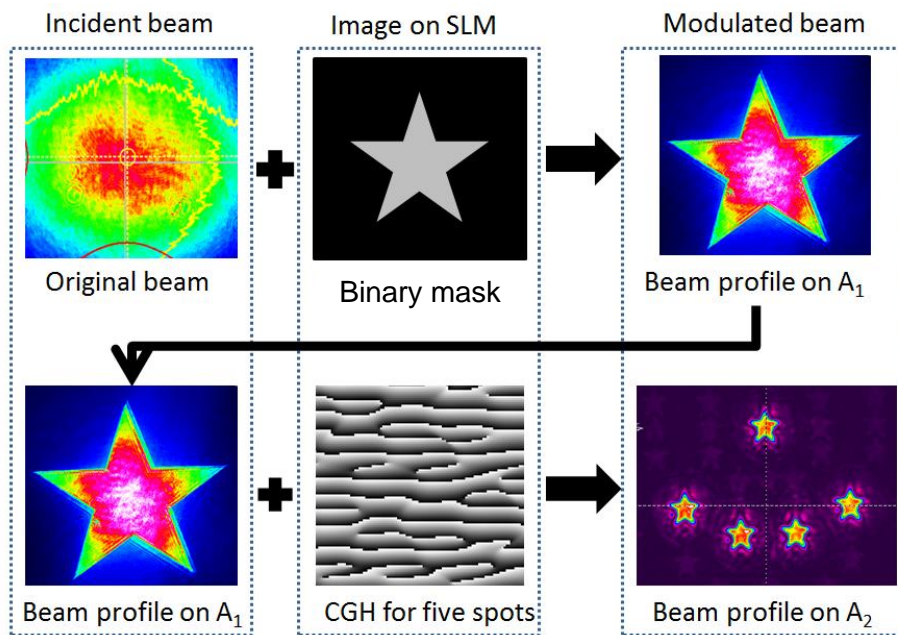


Figure 6 Five star shape beams. Top line: the original distribution plus a binary mask to achieve a star shape beam at  $A_1$ . Lower line: the square shape beam plus CGH to achieve five star beams at  $A_2$ . These still have non-uniform intensity as expected.

The advantage of using a grey level mask over binary mask is now demonstrated in achieving higher intensity uniformity. Figure 7 compares the results between using a binary mask and a grey level mask. Figure 7

(a) shows an output modulated by a binary mask and shaped into a square shape with intensity distribution similar to the original Gaussian distribution at both beam profilers  $A_1$  and  $A_2$ . In contrast, Figure 7 (b) shows an

output modulated by an appropriate grey level mask for achieving desired shape along with intensity uniformity. Thus, both the outline profile and intensity distribution are modulated and a square flat top beam has been created and separated into three

beams. It can be seen in figure 7 that the uniformity of flattop results on A2 is not as good as the results observed at A1. This is likely caused by knife-edge diffraction effects as the flattop beam is a diffracting beam.

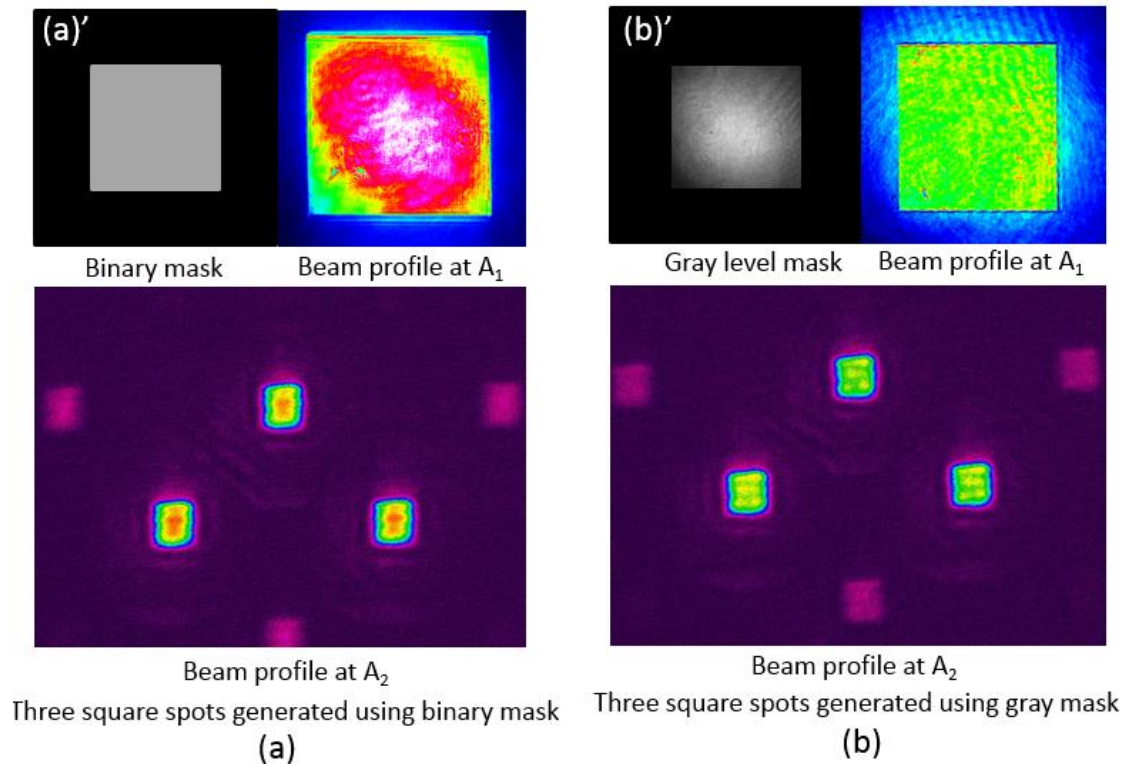


Figure 7 Comparison between a binary mask (a) and grey level mask (b) which creates more uniform intensity distribution. (a)' The centre of a binary mask with one continuous grey level (grey level =90) and (b)' the centre of a grey level mask with a grey level gradient (grey level: 0-255).

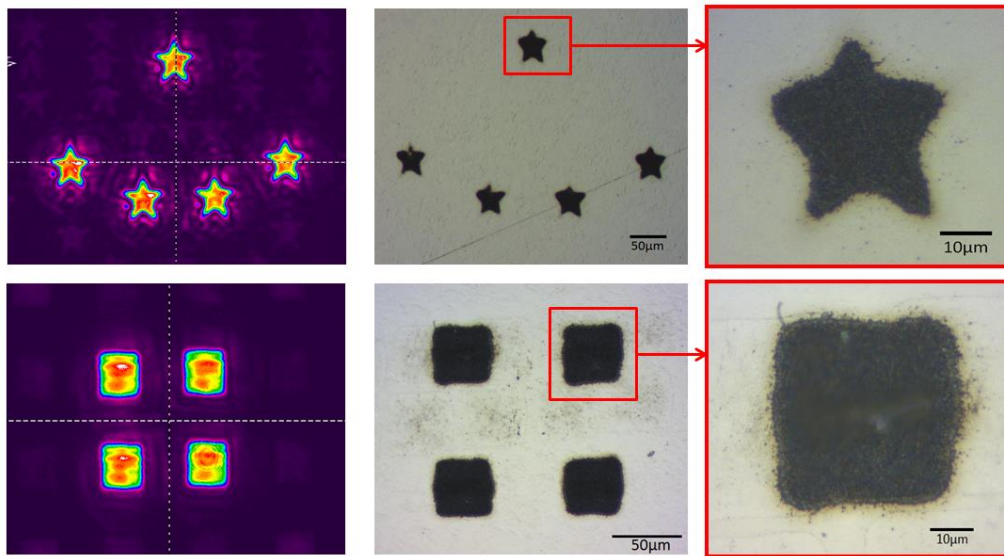
### 3.2 Picosecond Laser micro-machining results observed at image plane, A<sub>3</sub>.

Figure 8 shows the micro-machined footprints of multi beams with the shape of a star and a square. The beam was first shaped by a binary mask on SLM1, and then separated into multi beams using SLM2. Finally the beam reaches the F-theta lens and can be used for processing at the imaging plane of the optical system. Footprints were fabricated on a polished titanium sample. The input laser energy (E<sub>p</sub>) was approximately 10 μJ, measured before the scanning galvanometer aperture. Since

the laser frequency PRF = 10kHz and the drilling time for each pattern was 1s,  $\approx 10^4$  pulses were used to fabricate each footprint. As shown in Figure 8, the machined shape of footprints matched the observed beam profile very well. The side length of the square was 300pixel ( $\approx 1.94$ mm) and the magnification factor system was 1/45. Theoretically, the expected side length of the machined footprints was 43μm while the measured length of the footprints in the

bottom line of Figure 8 is approximately

40 $\mu\text{m}$ , very close to the calculated value.



Beam profile at  $A_2$

Machined patterns

Figure 8 Beam shaping with binary masks on SLM1 and machining results. First (top) line: profile of five stars and machined patterns. Second (bottom) line: profile of four squares and machined patterns. (10kHz, 10 $\mu\text{J}$ , 1s, fluence  $F \approx 0.19\text{J}/\text{cm}^2$ )

Surface profiles of footprints machined with both binary and grey level masks were measured using the white light interferometer (WYKO NT1100). As shown in Figure 9 (top), the footprints fabricated by binary masks showed an approximately Gaussian-shaped profile indicating that the inside beam intensity distribution was unshaped, as expected. On the other hand, the footprints fabricated by grey level mask showed much steeper side walls with a relatively flat bottom. This demonstrated a good match between the footprint shapes machined at the image plane at  $A_3$  and the

created beam shapes and intensity profiles observed at  $A_1$  and  $A_2$ .

The results produced by this method compare reasonably well to other SLM based methods of beam shaping [19, 20]. However edge definition and diffraction efficiency are currently lower. This is due to mask size and long beam propagation paths. The method presented in this work however is significantly more flexible and avoids complex CGH calculation. The beam shaping quality is depended on the mask size relative to the SLM and input beam dimensions and has been further investigated.

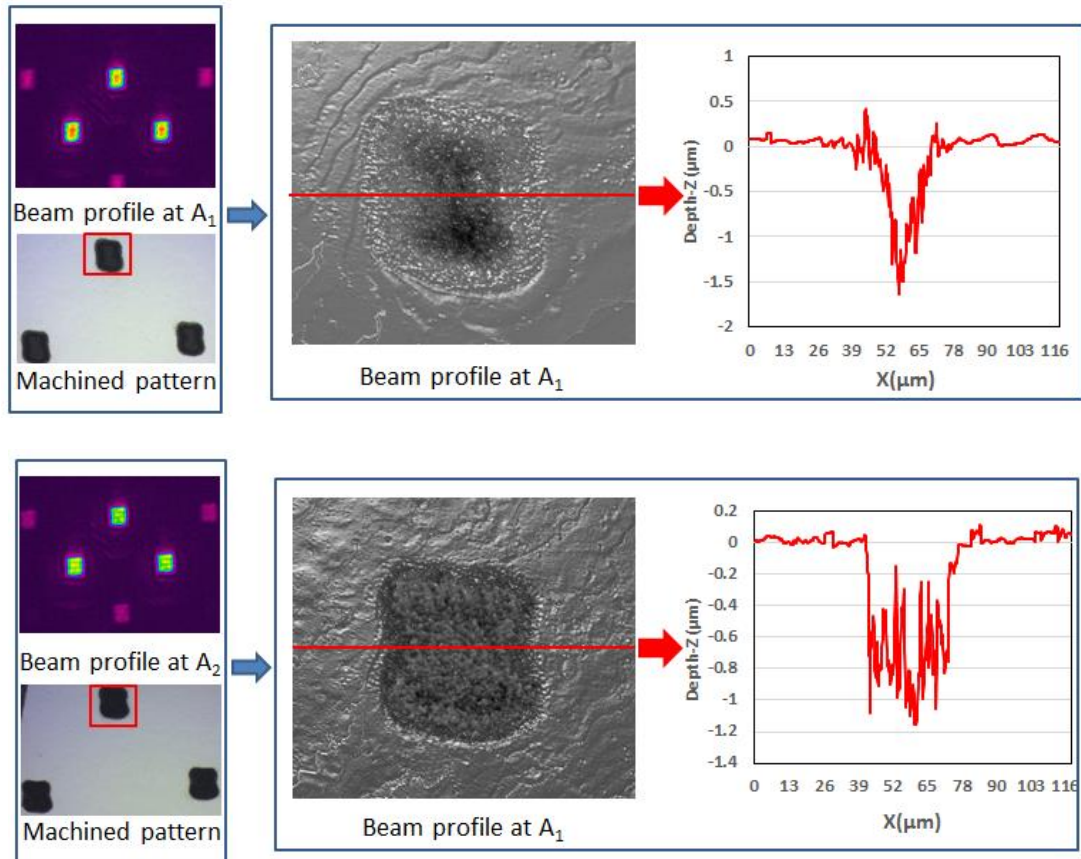


Figure 9. Comparison of laser machining results on polished Titanium using binary and 256 grey level masks. First (top) line: binary mask. Second (lower) line: grey level mask. (10kHz, 10 $\mu$ , 1s, fluence  $F \approx 0.19 \text{ J/cm}^2$ ).

### 3.3 Shaping efficiency versus the size of mask

In the process of beam shaping, a certain amount of energy will be blocked out due to the image applied on the first SLM. The shaping efficiency and quality may change when varying the size of the geometric mask. Figure 10 shows both binary and grey level mask shaped beam profile observed at  $A_1$  when varying the size of mask (side length varied from 150 to 500 pixels).

In order to quantitatively investigate the beam shaping efficiency and quality, images of the shaped beam profile observed at  $A_1$  were analysed by MATLAB. As shown in Figure 11, the grey level beam profile was read using MATLAB and each pixel was

varied from 0 (no power) to 1 (max power). The intensity value of a small area (3 $\times$ 3 pixels) can be seen in Figure 11. Accordingly, an entire shaped area matrix can be extracted. Shaping efficiency  $\eta$  can be calculated using the following equation,

$$\eta = \frac{\iint I_{shaped} dx dy}{\iint I_0 dx dy} \quad (9)$$

Where  $\iint I_{shaped} dx dy$  is the integral of the shaped beam intensity profile and  $\iint I_0 dx dy$  is the integral of the original beam intensity profile obtained at  $A_1$ . This calculation of efficiency is based on the real beam profile and carried out using MATLAB.

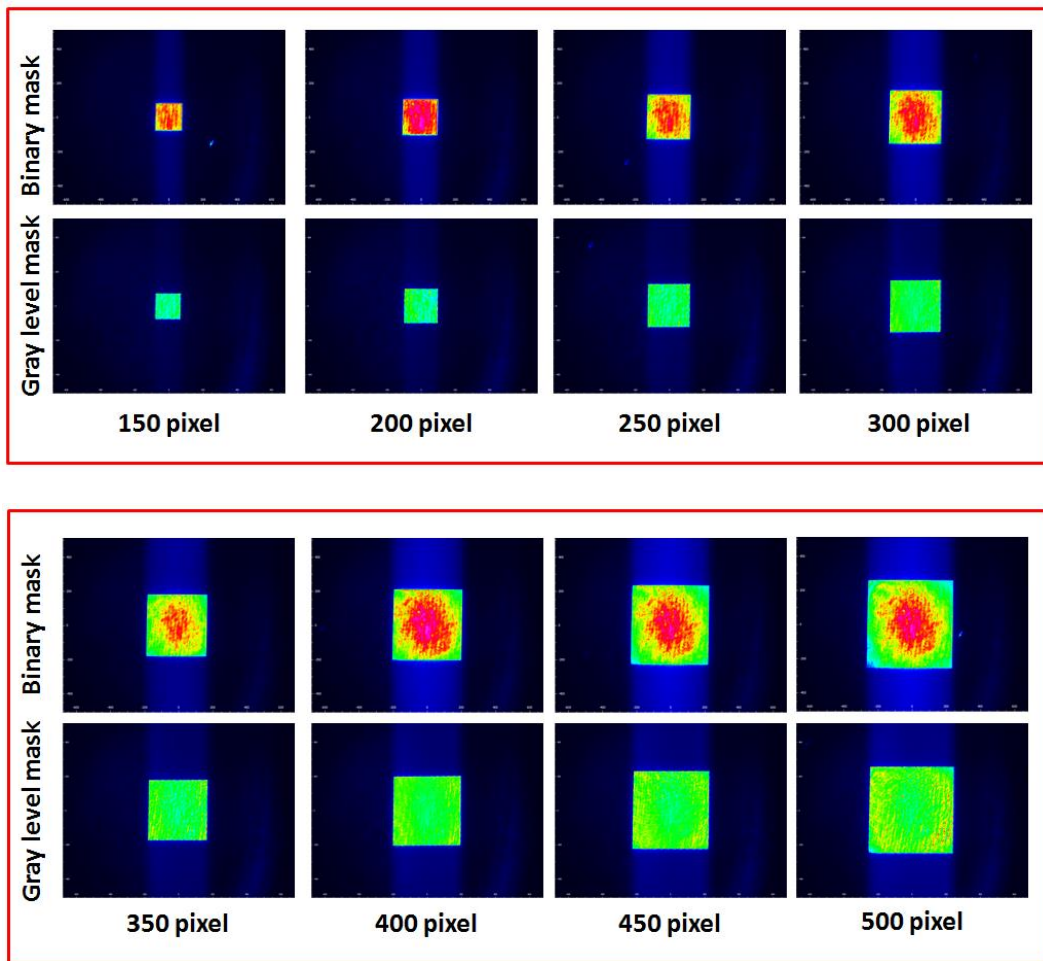


Figure 10 Beam shaping by binary and grey level mask through variation of mask size (side length of mask varied from 150 to 500 pixels).

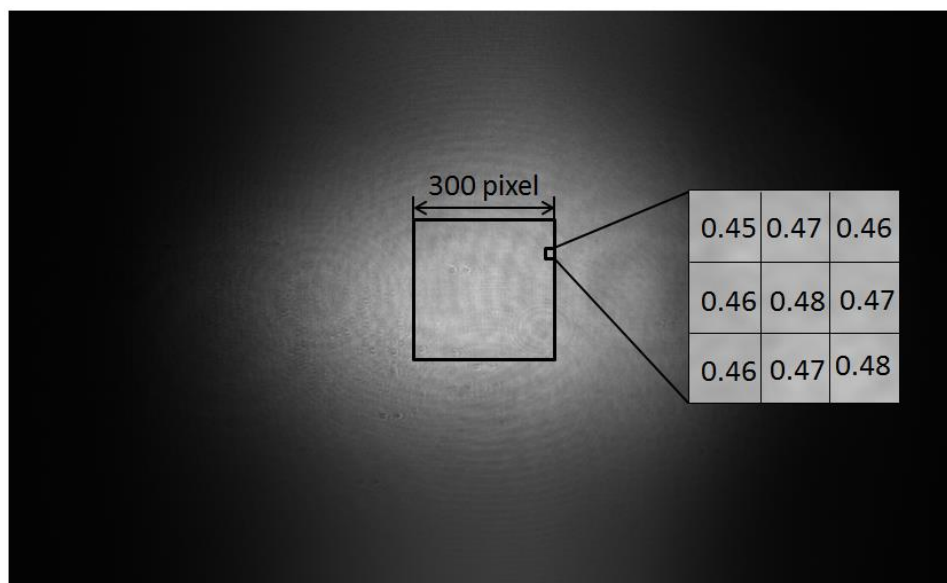


Figure 11 Analysis of Gaussian beam profile observed at  $A_1$  allowing the calculation of shaping efficiency and optimised grey level mask in Matlab to generate flat top intensity profile.

Figure 12 shows the comparison of shaping efficiency between the calculated value and measured value using a binary mask. The shaping efficiency becomes higher when the size of mask is larger as would be expected

as more of the original beam is being shaped and transmitted through analyser. The measured value is very close to calculated value, indicating good shaping quality and accuracy.

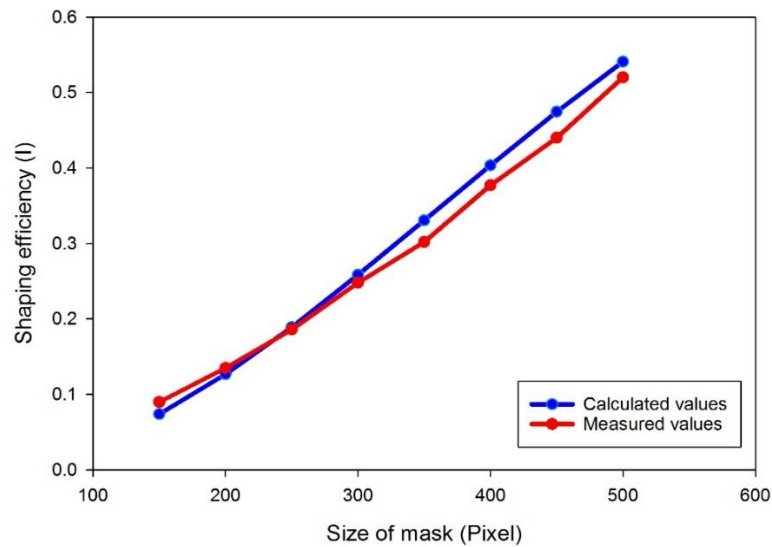


Figure 12 Calculated and measured shaping efficiency against the size of a binary mask.

Figure 13 shows the comparison between the calculated and measured shaping efficiency using a grey level mask. In this case, however, the measured values are consistently lower than the calculated values. This is likely due to the limitation of the

shaping ability of the SLM and the original distribution. As shown in Figure 14, when calculating the efficiency, a target intensity is chosen and all pixels in the shaped area are set as the target intensity.

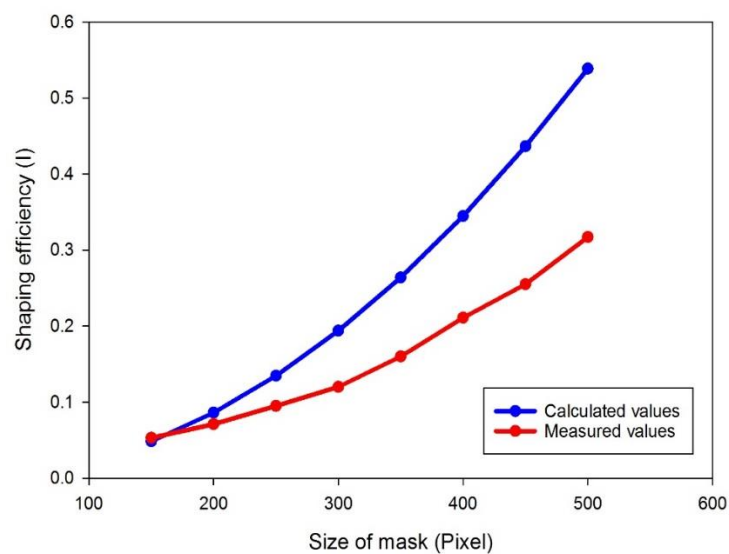


Figure 13 Comparison of calculated and measured shaping efficiency against the size of a grey level mask

It is clear that provided there is enough laser intensity most beam profiles can be produced. However if there is a limitation a balance between the shaped area and shaping quality must be found as the

shaping area cannot be over the limitation of the  $1/e^2$  of a Gaussian distribution. Therefore, the beam shaping limitation with this technique is dependent on the beam mode or  $M^2$  of the input laser.

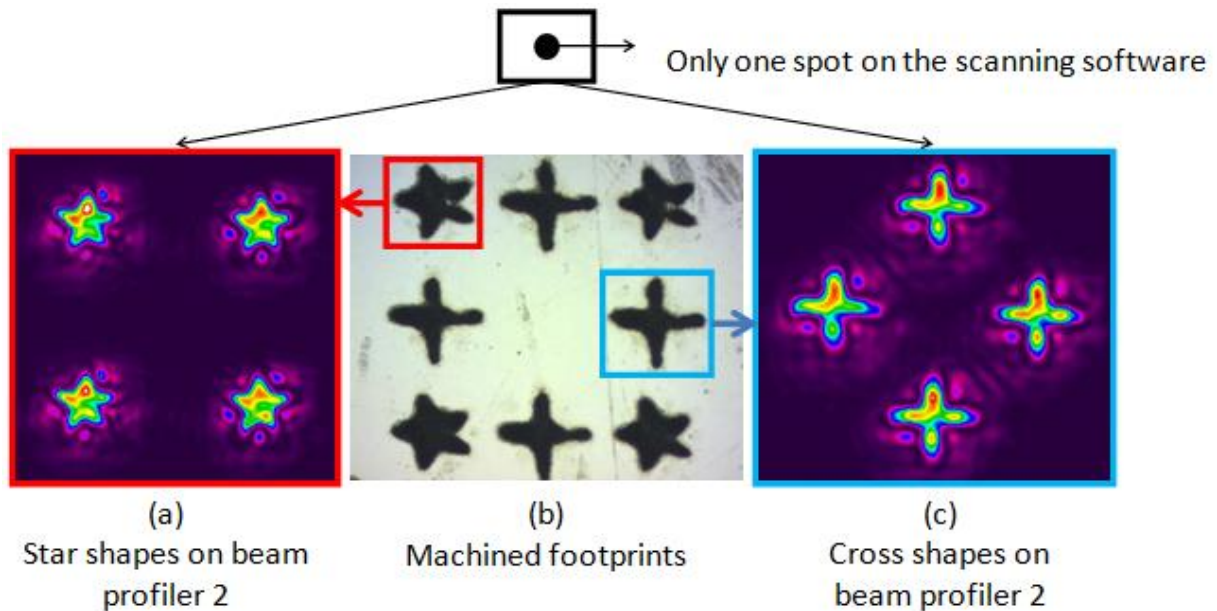


Figure 14 A combined pattern of stars and crosses created using multi beam shaping.

By applying two groups of holograms on the SLMs, complex machined footprints can be created as demonstrated in Figure 14b. The four star shapes (see Figure 14a) were generated and printed on the titanium sample first and then the four cross shapes (Figure 14c) machined afterwards. The shaping results indicate good flexibility of creating complex patterns with a relatively high efficiency.

#### 4 Conclusions

A novel ultrashort pulse laser beam-shaping technique to generate multiple geometric beams has been demonstrated. Binary and grey level masks applied on a spatial light modulator (SLM) were used to shape the outline profile and intensity distribution of the incident laser beam. After a long beam path, a second SLM was used to split the incident beam into multiple beamlets. A laser beam was effectively converted to

desired target shape, intensity distribution and separated pattern. A polished titanium sample was machined by the shaped beams at the imaging plane. The machined footprints have the corresponding shape and separated patterns closely matching those measured on intensity profilers. The size of the footprint can be adjusted by the mask and is comparable in size and slightly larger than the beam waist at the focal plane. The measured depth distribution on Titanium substrates also matches the designed intensity distribution very well. This technique can be potentially used for small size precision laser security marking on metals and semi-conductors due to the small footprints. Since both the outline profile and intensity distribution can be modified, it can be also used for removing a specific layer of material, such as thin film processing.

## References

- [1] C. Momma, B. Chichkov, S. Nolte, F. von Alvensleben, A. Tunnermann and H. Welling, "Short-pulse laser ablation of solid targets," *Opt Commun*, no. 129, pp. 134-42, 1996.
- [2] D. Vonder Linde and K. Sokolowski-Tinten, "The physical mechanisms of short-pulse laser ablation," *Appl Surf Sci*, no. 154-155, pp. 1-10, 2000.
- [3] S. Sundaram and E. Mazur, "Inducing and probing non-thermal transitions in semiconductors using femtosecond laser pulses," *Nat mater*, no. 1, pp. 217-24, 2002.
- [4] L. Sudrie, M. Franco, B. Prade and A. Mysyrowicz, "Study of damage in fused silica induced by ultra-short IR laser pulses," *Opt Commun*, no. 191, pp. 333-9, 2001.
- [5] S. Hasegawa, K. Shiono and Y. Hayasaki, "Femtosecond laser processing with a holographic line-shaped beam," *Optics Express*, vol. 23, no. 18, pp. 23185-23194, 2015.
- [6] T. Klerks and S. Eifel, "Flexible beam shaping system for the next generation of process development in laser micromachining," in *9th Int.Conf. on Photonic technique, LANE 2016 (Industrial Paper)*, 2016.
- [7] R. J. Beck, J. P. Parry, W. N. MacPherson, A. Waddie, N. J. Weston, J. D. Shephard and D. P. Hand, "Application of cooled spatial light modulator for high power nanosecond laser micromachining," *Optics Express*, vol. 18, no. 16, pp. 17059-17065, 2010.
- [8] F. Dausinger, "Machining of metal with ultrashort laser pulses: from fundamental investigation to industrial applications," *Proc. SPIE*, vol. 5777, p. 840, 2005.
- [9] M. Silvennoinen, J. Kaakkunen, K. Paivasaari and P. Vahimaa, "Parallel femtosecond laser ablation with individually controlled intensity," *Opt Express*, vol. 22, no. 3, pp. 2603-2608, 2014.
- [10] J. J. Kaakkunen, I. Vanttaja and P. Laakso, "Fast Micromachining Using Spatial Light Modulator and Galvanometer Scanner with Infrared Pulsed Nanosecond Fiber Laser," *Journal of Laser Micro/Nanoengineering*, vol. 9, no. 1, pp. 37-41, 2014.
- [11] H. Takahashi, S. Hasegawa, A. Takita and Y. Hayasaki, "Sparse-exposure technique in holographic two-photon polymerization," *Optics Express*, vol. 16, no. 21, pp. 16592-16599, 2008.
- [12] K. Fuse, "Beam Shaping for Advanced Laser," *Laser Technik Journal*, vol. 2, pp. 19-22, 2015.
- [13] C. Momma, S. Nolte, G. Kamlage, F. von Alvensleben and A. Tunnermann, "Beam delivery of femtosecond laser radiation by diffractive optical elements," *Appl.Phys.A*, vol. 67, pp. 517-20, 1998.
- [14] R. R. Thomson, A. S. Bockelt, E. Ramsay, S. Beecher, A. H. Greenaway and A. K. Kar, "Shaping ultrafast laser inscribed optical waveguides using a deformable mirror," *Opt Express*, vol. 16(17), pp. 517-20, 2008.

- [15] Z. Kuang, W. Perrie, S. Edwardson, E. Fearon and G. Dearden, "Ultrafast laser parallel micro drilling using multiple annular beams generated by a spatial light modulator," *JPhysD:Applphys*, vol. 47, p. 115501, 2014.
- [16] J. Li, Z. Kuang, S. Edwardson, W. Perrie, D. Liu and G. Dearden, "Imaging-based amplitude laser beam shaping for material processing by 2D reflectivity tuning of a spatial light modulator," *Applied Optics*, vol. 55, no. 5, pp. 1095-1100, 2016.
- [17] D. Liu, Y. Wang, Z. Zhai, Z. Fang, Q. Tao, W. Perrie, S. P. Edwardson and G. Dearden, "Dynamic laser beam shaping for material processing using hybrid holograms," *Optics & Laser Technology*, vol. 102, pp. 68-73, 2018.
- [18] Z. Kuang, J. Li, S. Edwardson, W. Perrie, D. Liu and G. Dearden, "Ultrafast laser beam shaping for material processing at imaging plane by geometric masks using a spatial light modulator," *Optics and Lasers in Engineering*, vol. 70, pp. 1-5, 2015.
- [19] J. M. Maxson, A. C. Bartnik and I. V. Bazarov, "Efficient and accurate laser shaping with liquid crystal spatial light modulators," *Appl.Phys.Lett*, vol. 171109, no. 105, pp. 1-5, 2014.
- [20] K. Osawa, M. Yoshida, Y. Nakata, N. Miyanaga and A. Narazaki, "Beam shaping by spatial light modulator and 4f system to square and top-flat for interference laser processing," *Proceeding of SPIE*, vol. 10091, pp. 1-8, 2017.